Controlling Nonlinear Normal Modes of Elastic Joint Robots

Master of Science Thesis

S. (Sahánd) Wagemakers

Presented for the degree of
Master of Science in Robotics

Delft University of Technology
To be defended on June 26, 2025 at 14:15

Supervisors:
Dr. C. (Cosimo) Della Santina
Dr. P. (Pietro) Pustina

Author: Sahánd Wagemakers
Student number: 4880897
Faculty: Mechanical Engineering
Department: Cognitive Robotics
Date: June 12, 2025

Controlling Nonlinear Normal Modes of Elastic Joint Robots

Sahánd Wagemakers, *Delft University of Technology*

***Abstract*—Through the use of Eigenmanifold theory, unforced periodic trajectories called nonlinear normal modes can be identified and excited in nonlinear mechanical systems. Applying this to repetitive tasks in robotic systems with elastic components can drastically reduce energy consumption, as normal modes in steady-state require no additional control effort. However, existing control methods for exciting nonlinear normal modes have so far only assumed full actuation. Consequently, these techniques are incompatible with series elastic joint robots, even though they represent a significant subclass of physical systems with elastic elements. Additionally, the calculation and parameterization of Eigenmanifolds for high-dimensional systems generally remains a complex task and is difficult to scale. While existing literature aims to avoid forced evolutions or model cancellation, we instead lean into this approach. By rephrasing Eigenmanifold-based control as a trajectory tracking problem, standard techniques for elastic joint robot trajectory tracking control can be employed. Furthermore, obtaining theoretical guarantees on global stability becomes possible. In this work, a new modular control architecture is presented that integrates trajectory tracking feedback control with Eigenmanifold theory to dynamically generate and track hyper energy-efficient oscillatory movements in underactuated systems. This approach enables the excitation of nonlinear normal modes using standard trajectory tracking controllers, while preserving energy-efficient properties desired from Eigenmanifold-based controllers. We first discuss the theoretical validity and energy-efficiency of this control architecture, and then test the architecture in simulation for a variety of use-cases and controllers.**

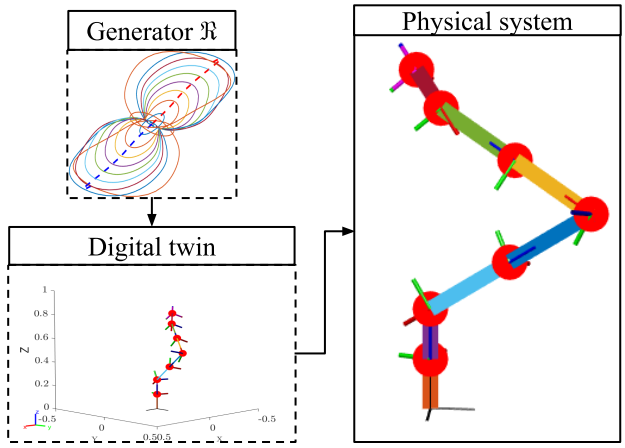

Fig. 1: By generating a reference through the real-time simulation of invariant evolutions of a virtual twin of the system, the two-layer control architecture allows for the use of any arbitrary trajectory tracking controller for energy-efficient nonlinear normal mode excitation.

I. Introduction

THE introduction of elastic elements into robotic systems instills compliant behaviors in their system dynamics, allowing for inherently safer environment interactions. This is especially beneficial for the design of robots that interact with humans, or operate outside of structured settings like labs and factories. In addition, since elastic elements are capable of storing and releasing energy, they can be exploited to reduce energy expenditure in periodic motions: by matching the task trajectory to the natural oscillations of the system, the task will require little energy to sustain. The concept of employing these ”natural motions” for the design of energy-efficient periodic trajectories has been extensively discussed and researched in the literature [1]. However, instead of considering natural motions for specific tasks, a more structured approach can be taken through the analysis and identification of nonlinear normal modes (NNMs). The study of NNMs deals with the identification and discovery of stable periodic evolutions of unforced nonlinear mechanical systems. While early definitions and research on NNMs date back to the 1960s [2], these initial frameworks are quite limited in their application, having been defined only for single-body systems [3]. The modern framework of Eigenmanifold theory [4] for the definition and identification of nonlinear modes is more general, allowing for modal analysis of multi-body systems. This makes the framework especially useful for robotic applications, which typically entail complex, multi-body systems.

The potential benefits of exciting NNMs to produce energy-efficient motions have already been demonstrated for a variety of robotic systems. In the case of pick-and-place tasks, the authors of [5] shape and excite NNMs to achieve directed point-to-point oscillations. Compared to regular PD control, the algorithms presented here use 99% less energy in the control task. Similarly, energy-efficient forward jumping movement is achieved for single-leg locomotion in [6], exploiting NNMs as trajectories in the stance phase. Experimental validation on the excitation of NNMs on has been performed on industrial manipulators in [7], providing the first step towards practical applications of Eigenmanifold controllers. Beyond energy-efficient control, Eigenmanifolds and modes can be used to obtain new insights into design and modeling. In [8], the accuracy of finite-dimensional representations of continuum soft manipulators is analyzed through the similarity of their Eigenmanifolds.

Though much literature is available on applications of NNM control in robotic systems [7, 6, 9, 10, 11], this collection of work is so far limited to fully actuated robotic systems. Exist-

ing Eigenmanifold controller pose NNM excitation as fulfilling a set of $n-1$ position constraints, $n-1$ velocity constraints and one energy constraint for an n-degrees-of-freedom (dof) robot. This phrasing of the problem is inherently difficult to apply to any underactuated system and assumes direct torque control, further limiting its application. Additionally, accurate knowledge of the Eigenmanifold is required, which becomes increasingly time-consuming and difficult to obtain for large-scale systems [7]. Besides this, existing stability proofs for Eigenmanifold controllers rely on locality assumptions and have so far not been extended to global stability [9, 12].

A significant portion of existing robots with elastic elements actively employ series elastic actuators (SEAs), either for locomotion [13, 14] or for compliant manipulators [15, 16]. To fully represent the dynamics of a SEA-driven robot, both the link- and motor-configurations and velocities need to be considered, resulting in a system that is underactuated by half the dofs. This presents a highly relevant open challenge: How can we excite NNMs of series elastic joint robots?

Generally, controlling nonlinear underactuated systems is a non-trivial problem for many robotic applications [17]. Solutions to the underactuated control problem are highly dependent on the exact dynamic properties of the system at hand, and thus require non-general solutions. However, it is well known that under common modeling assumptions, SEA-driven manipulators allow for the design of asymptotically stable trajectory tracking controllers through static feedback linearization [18, 19]. Since individual NNMs are essentially periodic trajectories of the system with special properties, this implies that for static feedback-linearizable systems, it is possible to regulate modal trajectories for both the actuated and unactuated configuration variables.

In this thesis, we synthesize existing knowledge on SEA-based control with Eigenmanifold theory through rephrasing the NNM control problem as a trajectory tracking problem, allowing for NNM excitation of underactuated mechanical systems. We introduce a modular, provably stable two-layer architecture that makes use of a digital twin and an Eigenmanifold generator for the dynamic generation of NNMs as smooth reference trajectories, and combines this with any compatible trajectory tracking controller. Figure 1 contains a visualization of the conceptual approach. Besides elastic joint systems, the two-layer architecture generalizes both to standard fully-actuated systems and closed-architecture fully-actuated robotic systems with no direct access to motor torque control. Furthermore, stability relies only on the trajectory tracking controller, meaning that if this subsystem is globally stable, so is the entire NNM excitation.

While this method does not aim to avoid dynamics cancellation or forced oscillations, as opposed to existing Eigenmanifold control methods, we show that the geometric and energy-efficient properties of Eigenmanifolds are fully preserved. The contributions of this thesis can be summarized as follows:

- A novel control architecture that allows for provably (global) stable excitation of NNMs without requiring a full representation of the Eigenmanifold.
- A reformulation of the Eigenmanifold-based NNM control problem as a trajectory tracking control problem that preserves the Eigenmanifold properties, allowing for NNM control for series elastic joint robots systems and fully-actuated (closed-architecture) systems.
- Theoretical and numerical validation of the control architecture on both simplified and realistic robotic systems.

Preliminary concepts and the problem specifications are introduced in section II. Then, the framework is presented in a general setting alongside more specific examples in section III. Numerical results are provided in section IV for an exact state-feedback linearizable subclass of underactuated mechanical systems called series elastic robots, and for a closed-architecture manipulator with joint-level trajectory control access.

To the best of our knowledge, this is the first work showing provably stable excitation of nonlinear normal modes of a class of underactuated mechanical multi-body systems, namely SEA-driven actuators. While the contribution relies mostly on existing theory on Eigenmanifolds and SEA-driven systems, the innovation of this thesis lies in the novel combination of these concepts in the proposed control architecture. By moving away from existing Eigenmanifold controller design principles and working around specific system limitations, we aim to provide a different perspective on how hyper energy-efficient control using NNMs may be achieved.

II. Dynamics & problem statement

While the focus of the thesis is on series elastic joint robots, Eigenmanifold theory has been developed with a broader applicability. Our goal is to design a control architecture which retains compatibility with previously studied systems, entailing fully-actuated conservative nonlinear mechanical systems. To account for both these cases, we first introduce the necessary background information in a more general sense. In future sections, we employ model-specific knowledge when discussing the individual sets of assumptions.

A. Model dynamics

Consider the general form of the conservative mechanical system

$$M(q)\ddot{q} + C(q,\dot{q})\dot{q} + G(q) = B(q)u, \tag{1}$$

where $q \in \mathfrak{X}$ denotes the system configuration on configuration manifold $\mathfrak{X} \subseteq \mathbb{R}^n$. Matrix $M(q) \in \mathbb{R}^{n\times n}$ is the positive definite inertia matrix, $C(q,\dot{q}) \in \mathbb{R}^{n\times n}$ is the Coriolis and centrifugal matrix, $G(q) = (\frac{\partial V(q)}{\partial q})^T \in \mathbb{R}^n$ collects the partial derivatives w.r.t. q of the potential energy $V(q) \in \mathbb{R}$. Matrix $B(q) \in \mathbb{R}^{n\times m}$ denotes the input coupling matrix, with input vector $u \in U \subseteq \mathbb{R}^m$ where U denotes the set of admissible inputs and $m \leq n$. A further assumption is made that this system contains a stable equilibrium point $(q,\dot{q}) = (q_{eq}, 0)$. The superscript ‘ ˙ ’ refers to a derivative with respect to time. We define a solution of the system as $(q(t), \dot{q}(t)) \in T\mathfrak{X}$, where $T\mathfrak{X}$ of dimension $2n$ is the tangent bundle of the configuration manifold.

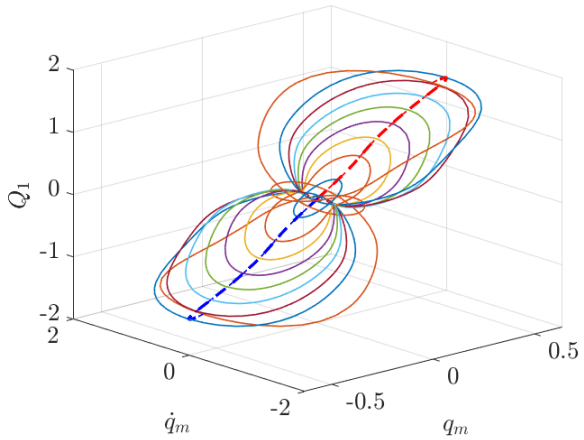

Fig. 2: A diagram of how the generator relates to the Eigenmanifold. The Eigenmanifold is a fibre-like structure of NNMs that extends from one of the two generators (portrayed in red and blue dotted lines).

In the following sections, we denote the energy of the system as

$$E(q,\dot{q}) = \frac{1}{2}\dot{q}^T M(q)\dot{q} + V(q). \tag{2}$$

When considering elastic joint robots, additional modeling assumptions are made, which are similar to the ones presented in [18]:

(A) The kinetic energy of the motor is only due to its own rotation.
(B) Inertial and gravitational effects are independent of the motor configuration and velocity.
(C) The elastic coupling between the motor and link is linear.

Under these assumptions, the equations of motion (1) now read

$$\begin{aligned} M(q_l)\ddot{q}_l + C(q_l,\dot{q}_l)\dot{q}_l + G(q_l) + K(q_l - q_m) = 0 \\ J\ddot{q}_m - K(q_l - q_m) = u, \end{aligned} \tag{3}$$

with joint link coordinates $q_l \in \mathbb{R}^m$ and motor link coordinates $q_m \in \mathbb{R}^m$. Together, they form the generalized coordinates $q = [q_l, q_m]^T \in \mathfrak{X}$. Matrix $G(q_l) \in \mathbb{R}^m$ contains potential effects only related to q_l such as gravity, and $K \in \mathbb{R}^{m\times m}$ is a positive definite diagonal matrix collecting the spring constants of the coupling between the motor and joint coordinates. Finally, $J \in \mathbb{R}^{m\times m}$ is the positive definite motor inertia matrix.

B. Eigenmanifolds and nonlinear normal modes

For linear conservative oscillatory systems with a state-space of size $2n$, any general evolution can be described as a sum of n linear normal modes (LNMs) [20, 21]. These LNMs are characterized by the properties of:

- *Invariance*: All LNMs are linearly independent, and thus orthogonal to each other.
- *Linear superposition*: Any general motion of the system can be described using a linear combination of the LNMs.

This definition of normal modes holds only for linear systems, as the linear superposition principle has no nonlinear equivalent. While multiple frameworks exist that aim to generalize this concept into the nonlinear domain [2, 3], only the framework of Eigenmanifold theory [4] is applicable to multi-body systems i.e. systems for which the mass matrix depends on q. Here, we introduce the necessary concepts for understanding Eigenmanifold theory and nonlinear normal modes expressed in the $(q,\dot{q})$ coordinates from (1). For a coordinate-free definition, we refer back to [4].

Within the context of Eigenmanifolds, a nonlinear normal mode (NNM) can be defined as follows.

Definition 1. (Nonlinear normal mode, adapted from [4]). An unforced solution $(q(t),\dot{q}(t)) \in T\mathfrak{X}$ of (1) is called a *Nonlinear normal mode* when $(q(t),\dot{q}(t))$ is

a. Periodic: There exists a $T \in \mathbb{R}^+$ such that $(q(t),\dot{q}(t)) = (q(t+T),\dot{q}(t+T))$.
b. Line-shaped: There exist a one-dimensional parameterization $\gamma(s)$ for $(q(t),\dot{q}(t))$, such that $s \in [0,1]$.

Together, specific collections of NNMs levels form smooth, two-dimensional manifolds called *Eigenmanifolds*. However, while Eigenmanifolds always consist of only NNMs, not every collection of NNMs is an Eigenmanifold. To obtain a precise definition, one can look at the construction of an Eigenmanifold, which is done using another geometric object called the generator. The generator $\mathfrak{R}$ is a 1-dimensional submanifold of $T\mathfrak{X}$ with the following properties:

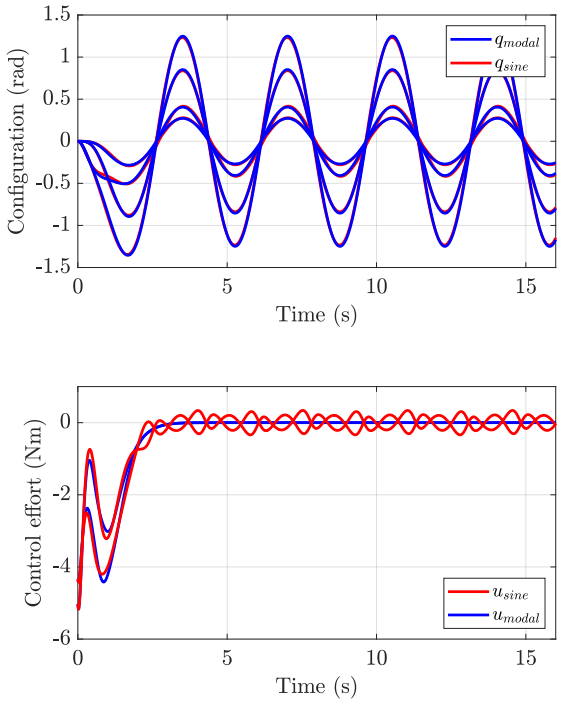

Fig. 3: Plots of the configuration and input torque for the tracking of an NNM and a smooth sinusoidal trajectory. Both have the same period and maxima, but the former requires no control effort at steady-state.

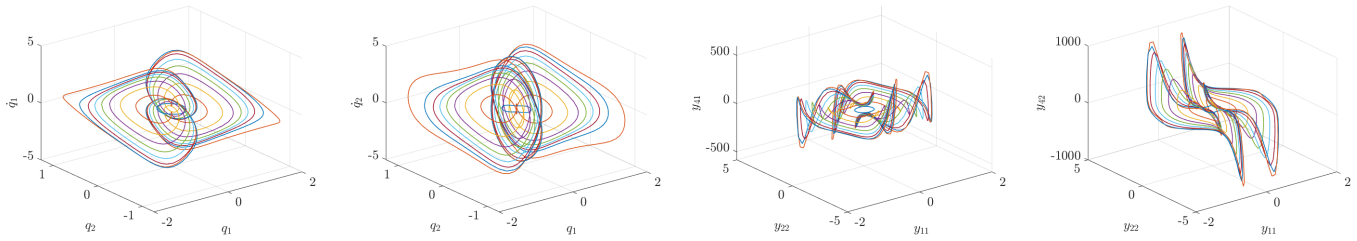

Fig. 4: Modes of an Eigenmanifold projected in different coordinates and state variables: $(q, \dot{q})$ state variables on the left and y state variables (see 16) on the right. The Eigenmanifold is identical, but may be expressed in various coordinate systems.

Definition 2. (Generator, adapted from [4]).
Consider the 1-dimensional connected submanifold $\mathfrak{R} \subseteq T\mathfrak{X}$ for system (1). This is called a generator if

- **a.** There exists a function $G(\mathfrak{R}) = \mathfrak{M}$ that constructs the 2-dimensional invariant manifold $\mathfrak{M}$.
- **b.** $\forall (q, \dot{q}) \in \mathfrak{R}$, then $\dot{q} = 0$.
- **c.** The generator contains only one unique equilibrium point $(q_{eq}, 0)$.

An important property is that a natural parameterization for the generator is the energy E. Using Definitions 1 and 2, the Eigenmanifold $\mathfrak{M}$ can then simply be defined as:

Definition 3. (Eigenmanifold, adapted from [4]).
Consider the 2-dimensional smooth invariant manifold $\mathfrak{M} \subseteq T\mathfrak{X}$ for system (1) that is constructed through $\mathfrak{M} = G(\mathfrak{R})$. This is called an Eigenmanifold if every evolution $(q(t), \dot{q}(t)) \in \mathfrak{M}$ is a nonlinear normal mode.

The coordinate expression of $\mathfrak{M}$ is then

$$\mathfrak{M} = \{(q, \dot{q}) \in T\mathfrak{X} | \exists \xi_m, s.t.\ Q(\xi_m) = q, \dot{Q}(\xi_m) = \dot{q}\}, \quad (4)$$

where $(Q(\xi_m), \dot{Q}(\xi_m))$ is the natural embedding of $\mathfrak{M}$ into the associated coordinates $(q, \dot{q})$ and $\xi_m \in \mathbb{R}^2$ is the parameterization of the Eigenmanifold. Numerous valid parameterizations ξ_m for the Eigenmanifold exist that can be either local or global. Figure 2 shows how NNMs, the generator and the Eigenmanifold are all related. The existence of at least n Eigenmanifolds emanating from the stable equilibrium of (1) are guaranteed. These Eigenmanifolds are essentially extensions of the n Eigenspaces of the linearized version of the system.
Due to the fact that NNMs are periodic invariant evolutions of the unforced system, no control effort is required to sustain them. These properties of invariance and periodicity can be exploited to design hyper-efficient controllers. Specifically, if one defines a control input that vanishes on the NNM, the mode will be self-sustaining once convergence is achieved. This makes the excitation of NNMs especially advantageous when tasked with repetitive point-to-point behaviors, as the energy consumption of the tracking effort is significantly reduced. An example is shown in Figure 3, where similar trajectories are tracked, but only the modal trajectory requires no control effort in steady-state.
Since Eigenmanifolds are geometrical objects, their properties are retained within any coordinate expression and under any change of coordinates. This is shown visually in Figure 4. More formally, we can write this as:

Corollary 1. *Given an Eigenmanifold $\mathfrak{M}$ of system (1) expressed in $T\mathfrak{X}$ through the natural embeddings $(Q(\xi_m), \dot{Q}(\xi_m))$. If there exists an invertible map $T : T\mathfrak{X} \to \mathbb{R}^{2n}$ in neighborhood U and $\mathfrak{M}$ is defined in this neighborhood, the natural embeddings $(Q(\xi_m), \dot{Q}(\xi_m))$ can be expressed in the new coordinate system as*

$$(T \circ Q(\xi_m), T \circ \dot{Q}(\xi_m)). \quad (5)$$

This implies that we can asymptotically force the system to the Eigenmanifold in any coordinate expression, and we can switch between the expressions by applying the change of coordinates to the Eigenmanifold embeddings. With the prerequisite knowledge introduced, we now specify the goals of the thesis.

C. Problem statement

We consider the Eigenmanifold control problem as a trajectory control problem. For both (1) and (3), we denote an arbitrary NNM as $(q_m(t), \dot{q}_m(t)) \in \mathfrak{M}$. We aim to find a controller $u = k(q, \dot{q}, q_m(t), \dot{q}_m(t))$ compatible with (1) and (3) such that

$$\begin{aligned} \lim_{t\to\infty} q &= q_m(t) \\ \lim_{t\to\infty} q &= q_m(t) \\ \lim_{t\to\infty} u &= 0. \end{aligned} \quad (6)$$

Essentially, this means that the proposed controller should require zero energy expenditure during the steady-state phase of the system. We avoid the pre-computation of NNMs as motion primitive trajectories, as this approach does not properly utilize the geometric properties that Eigenmanifold theory introduces. Finally, we assume perfect knowledge of the dynamics and system states.

III. Two-layer control architecture

When one considers any underactuated system such as an elastic joint robot, a new challenge appears: having full control over all system dofs cannot be guaranteed in general, as it entails dealing with a configuration space ($\mathfrak{X}$) with higher rank than the actuation space. Existing Eigenmanifold controllers frame the control task as controlling $n-1$ configuration constraints, $n-1$ velocity constraints and one energy constraint [4, 9, 11]. As such, this approach appears infeasible when considering systems that are not fully actuated.

Alternatively, we propose to tackle NNM excitation as a trajectory tracking problem. Existing literature on nonlinear systems [22, 19] discuss certain conditions under which a coordinate transformation exists such that a mechanical system may be fully feedback linearized, making trajectory tracking control possible. As elastic joint robots described through (3) fulfill these conditions [18], it follows that trajectory control is possible. While there is a wide array of existing methods for general underactuated control, such as underactuated backstepping [23], transverse orbital stabilization [24, 25], and sliding mode control [26], the feedback linearizability of elastic joint robots provides the main motivation to express Eigenmanifold control as a trajectory tracking task.

In the rest of this section, we present our two-layer control architecture. By considering NNM excitation as a trajectory tracking problem, we are able to separate control into a NNM generation task (general for nonlinear mechanical systems), and the trajectory tracking task, which is system- and actuator-specific. First, we employ a virtual system that is used to generate a reference trajectory of the selected NNM in real-time. Then, a trajectory controller with asymptotically convergent properties is used to track this reference. A schematic overview of the architecture can be found in Figure 5.

The two-layer architecture is modular and can be used with any reference trajectory controller. Thus, the architecture is compatible with both underactuated and fully actuated mechanical systems that permit such a controller. Although feedback linearization is used as a main motivator, other viable trajectory tracking methods, such as sliding mode control, can also be applied.

While this approach moves away from existing Eigenmanifold control methods, which focus on minimizing dynamics cancellation and forced evolutions, we believe the essential benefits of Eigenmanifold control are properly preserved. As discussed later in this section, the two-layer architecture relies on the geometric properties of the Eigenmanifold and NNM structure for trajectory generation and is able to achieve highly energy-efficient modal control.

We start with the following assumption:

Assumption 1. *Suppose there exists a change of state variables $\theta = h(q, \dot{q})$, such that the dynamics* (1) *turn into*

$$\dot{\theta} = f(\theta) + g(\theta)u \tag{7}$$

where θ can be controlled to be

$$\lim_{t\to\infty} \theta = \theta_d, \tag{8}$$

for any arbitrary desired state θ_d.

Note that under this assumption, we do not put any restrictions on the (non-)linearity of $\dot{\theta}$. Rather, we state that a base requirement is that there exists a controllable system (θ) which is feedback equivalent to $(q, \dot{q})$. In the case of a fully-actuated system, this change of state variables is the identity $\theta = [q, \dot{q}]^T$. In the case of an elastic joint robot, the change of state variables denotes the link position, velocity, acceleration, and jerk. This will be discussed in more detail in subsection III-B.

We provide an elementary definition for feedback equivalence as a one-to-one invertible transformation between $g(\theta)u$ and $B(q)u$ over the same time interval (t_b, t_e). A formal definition of feedback equivalence can be found in [27].

Next, we discuss the two layers of the control architecture.

A. Trajectory generation through virtual dynamics

Generating a valid trajectory $\{(q_d(t), \dot{q}_d(t)) \in \mathbb{R}^{2n}, t \in [t_b, t_e]\}$ for an underactuated system requires that it is a viable solution of the system dynamics. This means that the reference trajectory should not only be smooth, but also have an associated control sequence $\{u(t), t \in [t_b, t_e]\}$ that is within the span of permissible inputs $u(t) \in U$. This is always the case for an NNM, as the associated control sequence is the trivial zero control $u(t) = 0$ for the entire trajectory. While trivially proven, this is a relevant property for the trajectory generation, and is thus formally written down as the proposition below.

Proposition 1. *Any NNM $(q_m(t), \dot{q}_m(t)) \in \mathfrak{M}$ is a viable solution of* (3) *or* (1) *with any arbitrary input coupling matrix $B(q) \in \mathbb{R}^{n\times m}$.*

While it is possible to parameterize the NNM trajectory using time, this requires precomputing an accurate parameterization of the desired mode. If the goal is to control a variety of NNMs for high-dimensional systems, this needs to be done for each mode. Given that high energy NNMs do not necessarily resemble sinusoids, choosing the right parameterization for each energy level can be challenging. When a closed form of the entire Eigenmanifold is necessary, the task becomes even more difficult and time-consuming. In [7], a point cloud-based Eigenmanifold construction and control strategy was designed to explicitly avoid dependence on a closed parameterization of the Eigenmanifold, as this is believed to be more feasible for higher-dimensional systems. Either way, the requirement of having a full, accurate estimate of the Eigenmanifold is nontrivial for large systems.

Instead, recall that Eigenmanifold $\mathfrak{M}$ is invariant, so any open-loop solution that starts on the Eigenmanifold will stay there indefinitely. Since we only consider conservative systems, the solution $\{(q_d(t), \dot{q}_d(t)), t \in [0, \infty], (q_d(0), \dot{q}_d(0) \in \mathfrak{M})\}$ will track the NNM of Eigenmanifold $\mathfrak{M}$ at energy level $E(q_d(0), \dot{q}_d(0))$.

Thus, the reference trajectory can be computed in real-time by integrating the dynamics (1) starting from any state on the Eigenmanifold with the desired energy level. This digital twin of the dynamics will be referred to as the *virtual system* with state $(q_d, \dot{q}_d)$.

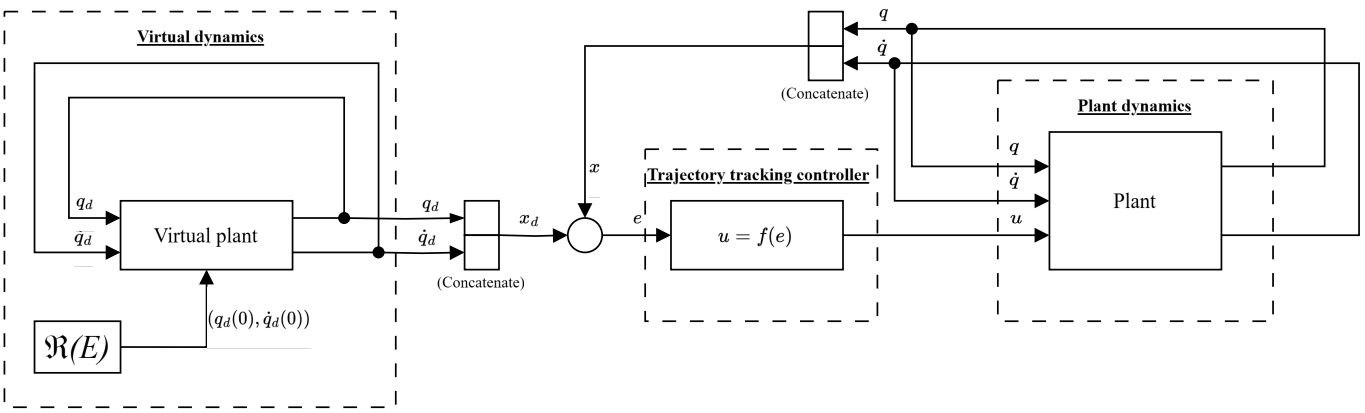

Fig. 5: Schematic representation of the two-layer architecture. The trajectory tracking sub-diagram is interchangeable for any arbitrary reference trajectory tracking controller.

To select the initial state, we use the generator $\mathfrak{R} \subset \mathfrak{M}$ used to construct the Eigenmanifold. Since $\mathfrak{R}$ can be parameterized by energy E, an initial state $(q_d(0), \dot{q}_d(0) = 0) \in \mathfrak{R}_Q(E)$ will result in the desired reference trajectory. Here, $R_Q(E) \in T\mathfrak{X}$ denotes the coordinate expression of $\mathfrak{R}$ in state space $(q, \dot{q})$ parameterized by energy E.

Generating a reference trajectory of the desired NNM through the virtual dynamics only requires us to know the model dynamics and the generator $\mathfrak{R}$ of $\mathfrak{M}$. Thus, we do not require a parameterization of the full Eigenmanifold. While the virtual system requires accurate knowledge of the system dynamics, this is not more restrictive compared to other Eigenmanifold controllers, since the calculation of $\mathfrak{M}$ depends on a similarly high level of accuracy. Under a model parameter mismatch, periodic oscillations are still excited, but the steady-state control effort will not fully converge to zero [9].

B. Trajectory tracking

Under Assumption 1 and Proposition 1, we can claim that there exists a controller that can asymptotically converge the system state to $((q_d(t), \dot{q}_d(t)) \in \mathfrak{M}$. Furthermore, the energy-efficient properties are similar to other Eigenmanifold controllers. These facts are as follows.

Lemma 1. *Consider system* (1) *and suppose Assumption 1 holds. Then, any NNM* $(q_d(t), \dot{q}_d(t)) \in \mathfrak{M}$ *of can be asymptotically stabilized as*

$$\begin{aligned} \lim_{t\to\infty} q &= q_d \\ \lim_{t\to\infty} \dot{q} &= \dot{q}_d. \end{aligned} \tag{9}$$

Additionally,

$$\lim_{t\to\infty} u = 0. \tag{10}$$

Proof. Using corollary 1, we may transform $(q_d(t), \dot{q}_d(t))$ to

$$\theta_d = h(q_d, \dot{q}_d(t)). \tag{11}$$

As assumption 1 tells us of the existence of v such that $\lim_{t\to\infty} \theta = \theta_d$, we can then apply the inverse transformation h^{-1} to obtain

$$\begin{aligned} &\lim_{t\to\infty} h^{-1}(\theta) = h^{-1}(\theta_d) \\ &= (\lim_{t\to\infty} q = q_d, \lim_{t\to\infty} \dot{q} = \dot{q}_d). \end{aligned} \tag{12}$$

Now, casting this into the full equations of motion (1) results in

$$\lim_{t\to\infty} M(q_d)\ddot{q}_d + C(q_d, \dot{q}_d)\dot{q}_d + G(q_d) = B(q_d)u. \tag{13}$$

Due to the uniqueness of solutions to the Cauchy problem, we know that there is only one valid solution for $q = q_d, \dot{q} = \dot{q}_d$, which is

$$M(q_d)\ddot{q}_d + C(q_d, \dot{q}_d)\dot{q}_d + G(q_d) = 0 \tag{14}$$

as $(q_d(t), \dot{q}_d(t)) \in \mathfrak{M}$. Since $B(q, \dot{q})$ is not the trivial zero matrix, this means

$$\lim_{t\to\infty} u = 0, \tag{15}$$

concluding the proof. □

Lemma 1 tells us that the control effort of any arbitrary trajectory tracking controller must go to zero if the reference trajectory is an NNM. Thus, the property of energy-efficiency is guaranteed for any choice of trajectory tracking controller using the two-layer control architecture.

Elastic joint robots

For SEA-driven manipulators described by (3), it is well established [18] that there exists a change of state variables $T_y : T\mathfrak{X} \to \mathbb{R}^{2n}$ from $(q, \dot{q})$ to $y = [y_1, y_2, y_3, y_4]^T$

$$\begin{aligned} y_1 &= T_{y1}(q, \dot{q}) = q_l \\ y_2 &= T_{y2}(q, \dot{q}) = \dot{q}_l \\ y_3 &= T_{y3}(q, \dot{q}) = \ddot{q}_l \\ y_4 &= T_{y4}(q, \dot{q}) = \dddot{q}_l \end{aligned} \tag{16}$$

which fulfills Assumption 1. Within these coordinates, we can design asymptotically stable trajectory tracking controllers

such as a pole-placement controller through feedback linearization, which is defined as

$$\begin{aligned} u =& - JK^{-1}M(q_l)F(q,\dot{q}) + JK^{-1}M(q_l)v \\ v =& \ddot{y}_{d4}(t) + k_1(y_{d1}(t) - y_1) + k_2(y_{d2}(t) - y_2) \\ &+ k_3(y_{d3}(t) - y_3) + k_4(y_{d4}(t) - y_4) \end{aligned} \tag{17}$$

where $F(q,\dot{q})$ collects all terms of $\ddot{q}_l$ not related to u. The scalars $[k_1, k_2, k_3, k_4]$ are strictly negative gains chosen such that the eigenvalues of $\dot{y}$ are negative definite and $y_d(t) = T_y \circ (q_d(t), \dot{q}_d(t))$ denotes the modal trajectory expressed in the y coordinates. Note that instead of (17), other controllers such as sliding mode control may also be used. The controller derivations of these two examples are left out of the main thesis body and are instead presented in Appendix A, as they do not contain any novel knowledge.

(Closed-architecture) fully actuated manipulators

As the two-layer architecture only requires the existence of a converging trajectory tracking controller, this method can also be applied to fully actuated systems. In this case, the transformation $h(q,\dot{q})$ described in assumption 1 simply denotes the identity transform I. This is particularly useful when dealing with a robotic system using a closed control architecture. For closed architecture systems, it is only possible to send commands to the robot through input channels provided by the manufacturer. If these channels do not include torque control, existing manifold controllers cannot be used. However, as long as there is access to a trajectory tracking controller, the two layer architecture can be employed while preserving the energy-efficient properties that are desired when using modal control. For example, if a closed architecture robot provides a simple PID joint controller defined as

$$\begin{aligned} u =& K_p(q_d(t) - q(t)) + K_d(\dot{q}_d(t) - \dot{q}(t)) \\ &+ K_i \int_0^t (q_d(\tau) - q(\tau))d\tau \end{aligned} \tag{18}$$

with access to the scalar gains K_p, K_d, K_i and reference input $q_d(t), \dot{q}_d(t)$, Lemma 1 still holds true as long as the gains are chosen such that the trajectory tracking controller is asymptotically convergent.

C. Extension to other classes of underactuated systems

Looking at Assumption 1 and Lemma 1, there is the implication that the two-layer architecture may be applied on any underactuated system that permits both an Eigenmanifold and a trajectory tracking controller. An example of such a system is an planar n-dimensional joint robot with $n \geq 3$ where the last link is unactuated. For such a system, it is known that trajectory tracking control can be designed with a combination of partial feedback linearization and dynamic feedback linearization [28]. Do note that the introduced coordinate transformation is local, and thus does not have any global convergence guarantees. However, the question is raised whether this larger class of underactuated systems extends beyond elastic joint robots far enough to have any relevant or practical applications. Nonetheless, while a formal proof for the system introduced in [28] is beyond the scope of this work, we provide a small set of initial simulations to back up our claim in section IV. In this section, we also consider the cases of the elastic joint manipulator and fully actuated PID joint controller in simulation to verify whether numerical results match the theoretical performance.

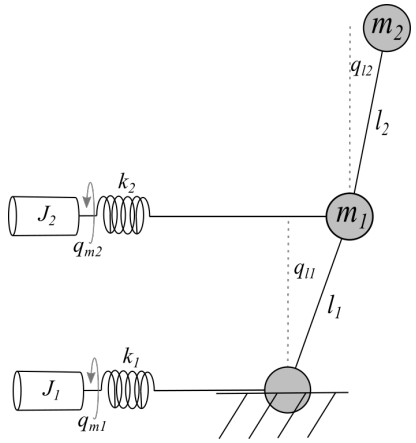

Fig. 6: The planar double pendulum with series elastic actuators.

IV. Numerical validation

To validate the theoretical results provided in the previous section, we consider the example cases of the elastic joint manipulator and fully actuated PID joint controller in simulation. The goal is to show the properties of global asymptotic stability, scalability to larger systems, and modularity of the system through numerical simulation. While not the main contribution of this thesis, energy-efficiency and modal switching are also considered, as they are important motivations for exciting NNMs in mechanical systems.

In total, three case studies are considered: a series elastic actuated double pendulum, a 6-degree-of-freedom manipulator with series elastic joints and a fully actuated closed-architecture 6-degree-of-freedom manipulator with rotational springs located in the joints. The equations of motion used for simulation and the Eigenmanifold calculation are obtained analytically for the double pendulum and numerically for both the 6-degree-of-freedom manipulators. In addition to the three main case studies, we provide some initial results on modal excitation of a planar manipulator model as described in [28] with additional parallel springs.

In the fully-actuated simulation, a comparison is made with the PD-like modal controller of [9]. This comparison cannot be made in the other simulations, as existing Eigenmanifold-based controllers are not designed for application to underactuated systems. The considered Eigenmanifolds are assumed to be prolongations of the Eigenspace of the linearized system around the equilibrium. To calculate the generator, an implementation of the procedure described by [29] in *Matlab2022b* is used. For validation of the virtual system dynamics, the full Eigenmanifolds embeddings are estimated by a 5x5 2-dimensional polynomial surface fit using the *sfit* function. Note here that depending on the complexity of the Eigenmanifold,

either a higher or lower degree polynomial fit may be more effective. In the case studies, we aim to present a variety of modes of various Eigenmanifolds at different energy levels. For all simulations, the gravity constant is set to be $g = [0, 0, 9.81]^T \ m/s^2$ described in 3-dimensional Euclidean space.

Simulation 1: Series elastic actuated double pendulum

Physical model: We consider a planar double pendulum with series elastic actuated joints such that $n = 4$. The system's physical parameters are found in Table I. The coordinates are set up such that $q_{eq} = [0, 0, 0, 0]^T$ denotes the stable equilibrium configuration with a potential energy $E(q_{eq}, 0) = 0 \ J$. A visual representation of the system is displayed in Figure 6.

TABLE I: Physical parameters of double pendulum.

Link	1	2
Mass (kg)	1	1
Length (m)	1	1
Motor inertia $(kg\ m^2)$	1	1
Motor stiffness (N/m)	10	10

Controllers: To show the modularity of the two-layer control architecture, two different trajectory tracking controllers are used: exact state-feedback linearization [18] (FFL) and sliding-mode control [30] (SMC), which are both generally accepted control methods for trajectory tracking of elastic joint manipulators.

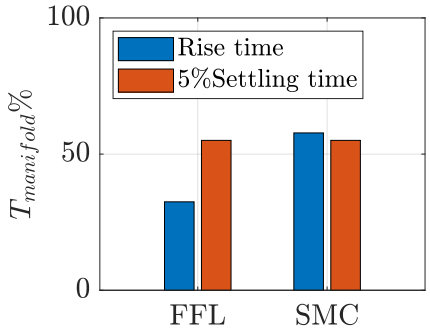

(a) Average joint rise time and settling time.

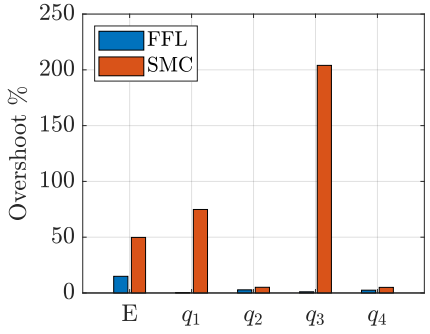

(b) Average energy and joint overshoot.

Fig. 7: Performance metrics for simulation 1.

General performance: In Figure 7, numeric performance metrics of the controllers starting from the equilibrium state are presented. The metrics are collected and averaged over the excitation of a range of modes with energy levels from $E = 1J$ to $E = 15J$. To gain more insight into the relative performance of the modes itself, the rise time and settling time are presented as relative percentages of the NNM period. Including some variance between controllers, rise times and settling times of about half a modal period can easily be achieved. More interestingly, sub-figure 7b shows a large difference in relative overshoot between SMC and FFL control. While there was no simulation in which convergence to the desired mode did not occur for either controller, this does imply that general performance is still highly dependent on the selected reference controller. These differences in performance are also apparent in Figure 8, which shows excitation from the equilibrium for modes around $E = 10J$ of the system Eigenmanifolds. As expected, while the transient state is unpredictable, asymptotic convergence to the NNM is clearly achieved. However, a limitation of the naive implementation of the two-layer architecture is seen in the excitation of manifold 3: due to a high initial distance from the reference trajectory in state-space, the controller input starts with infeasible input actions. We believe that this can be improved either through controller gain tuning, or first exciting lower energy modes and then slowly increasing the desired energy.

Global stability: To verify global convergence, 256 simulations are performed from randomly sampled initial conditions within the interval $q(0) \in [-0.5\pi, 0.5\pi], \dot{q}(0) \in [-0.25\pi, 0.25\pi]$ for a specific energy level $E = 1J$. While this sampling space does not encapsulate the theoretical full state space, we believe this to be a sufficiently large interval to capture a wide variety of initial conditions. The Euclidean norm $||q - q^{mi}(t)||$ of the error is presented in Figure 9 for both the FFL and SMC controller. While there is a clear variance in error over time, the eventual asymptotic convergence is consistent over all individual simulations. As the period for the selected Eigenmode is around $T = 1.2s$, the error only truly disappears after multiple oscillations. It is expected that more aggressive controller tunings might decrease the convergence time, but doing so would be at the expense of required input torque. Similar results were achieved for different Eigenmanifolds and energy levels. As we are primarily interested in verifying whether the energy consumption goes to zero when asymptotically close to the reference trajectory, the input torque is considered when at a steady-state. The control effort for both FFL and SMC, as seen in Figure 8, converges to zero as the modal trajectory is successfully tracked, validating the theoretical findings of the previous section.

Modal switching: Without requiring any additional implementation work, modal switching can be performed by resetting the state of the virtual system to a state on the generator at the new desired energy level. Checking whether we are nearby the generator is easily done by looking at the total system velocity, which is only zero on the generator. To test this, the simulation is initialized from the equilibrium, and the desired energy is increased every 12 seconds. To save

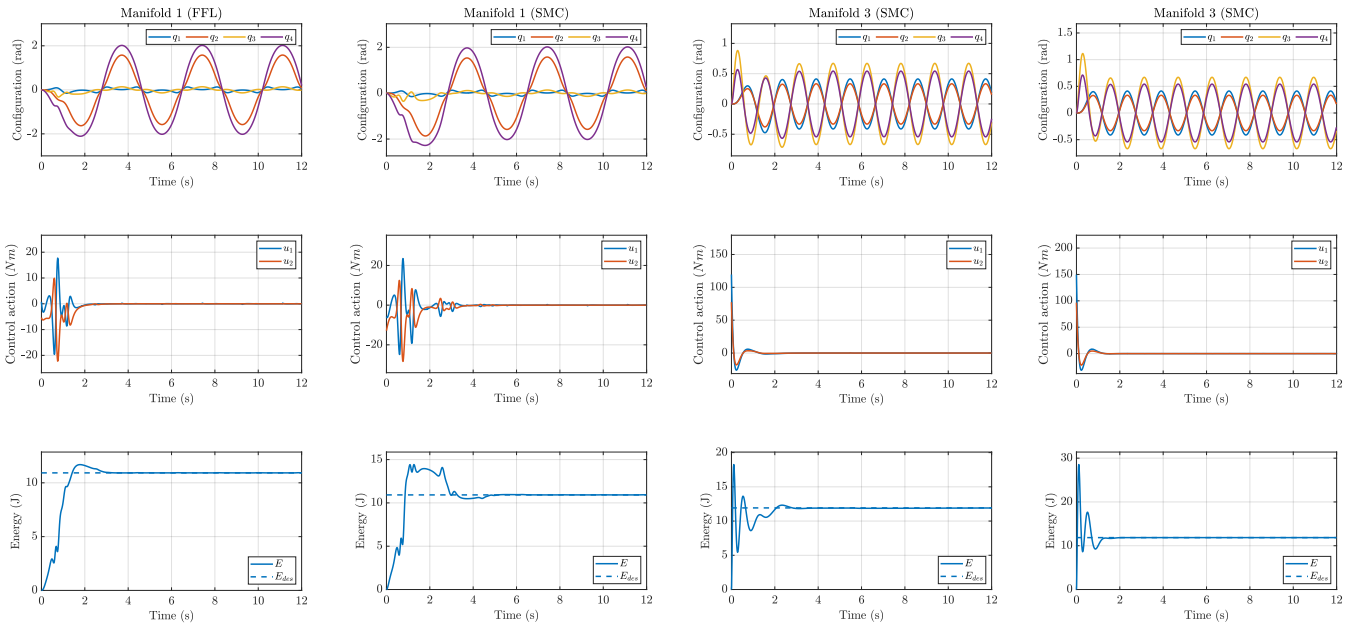

Fig. 8: Excitation of the Eigenmanifolds of the double pendulum with desired energy $E = 10J$ for each of the system manifolds, starting from the equilibrium position.

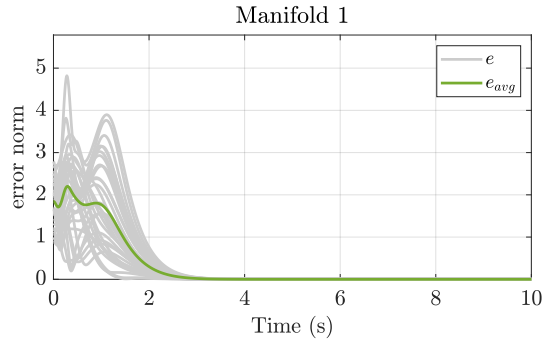

(a) FFL

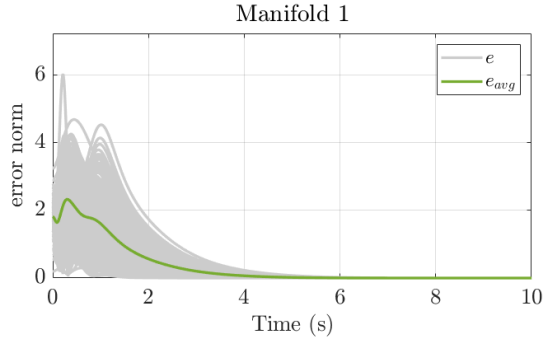

(b) SMC

Fig. 9: average error of the configuration over time for a mode of $E = 1J$ of the first Eigenmanifold.

space, we only discuss the results of Eigenmanifold 1 in Figure 10.

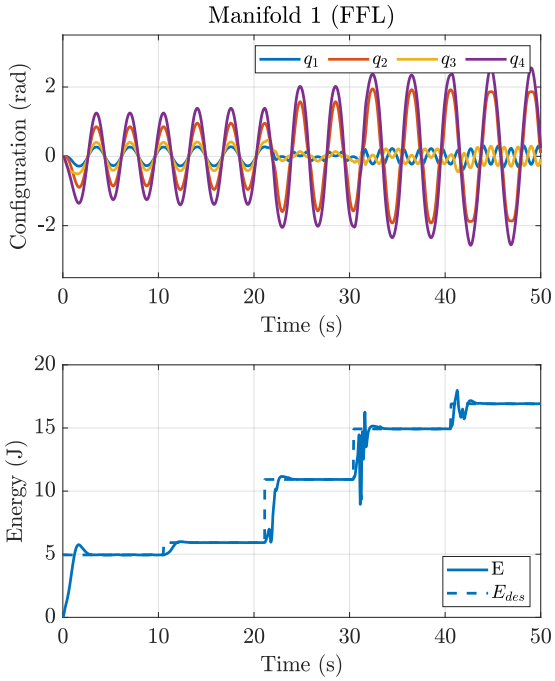

Fig. 10: Modal switching of the first Eigenmanifold for simulation 1.

Simulation 2: 6-dof series elastic actuated manipulator

We show how the control architecture may be applied to more realistic systems without severely impacting performance or scalability. Due to the complexity of the system, the equations of motion are derived numerically. Nonetheless, results are similar to the theoretically perfect case. Since the goal of this section is to show whether the system may be scaled up

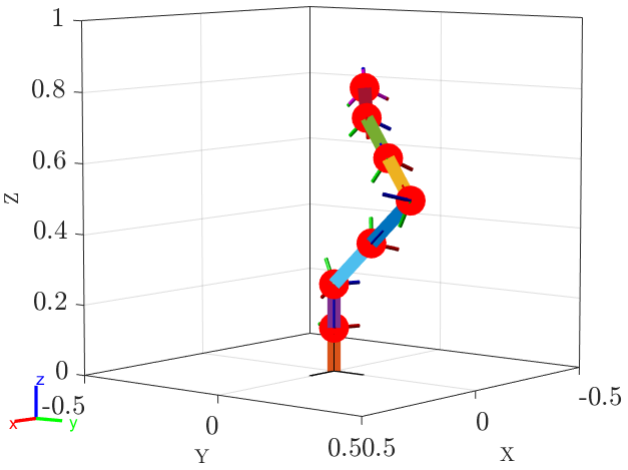

Fig. 11: An image of the 6-dof manipulator in Matlab. The same design is used for both the series-elastic actuated and stiff joint experiments.

rather than to revalidate the results of the double pendulum system, we will only discuss the general performance and modal switching on a single Eigenmanifold.

Physical model: The manipulator is tested with joint stiffnesses ranging between $50Nm/rad$ and $850Nm/rad$, which is based on feasible joint stiffness range used in physical elastic joint robots [31]. Virtual parallel torsion springs on the motor joints are modeled to allow for selection convex energy minimum at a larger range of manipulator configurations. This virtual spring stiffness is selected to be $k_{vspring} = [30, 30, 20, 20, 20, 15]Nm/rad$, which is around 5-10% of the elastic link torsional stiffness. The justification for the virtual spring is the expectation that a manipulator will be tasked with point-to-point operations which might not include the true convex potential energy minimum. The virtual spring allows us to manipulate the local energy minimum and is easily implementable through an additional control action on the motor link. The exact parameters used can be found in Table II. Here, we provide the motor inertia of each joint as the diagonal entries of J as described in (3), meaning $J_i = m^2_{motor\ i} * I_{motor\ i}$. The equations of motion are obtained by the *Robotics System Toolbox*. An image of the workspace can be found in Figure 11.

TABLE II: Physical parameters of the 6-dof manipulator.

Link	1	2	3	4	5	6	7
Mass (kg)	2	1	1	1	0.5	0.5	0.5
Length (m)	0.125	0.125	0.25	0.25	0.25	0.25	0.125
Inertia $(kg\ m^2)$	0.5	0.5	0.5	0.5	0.5	0.5	**x**
Stiffness (Nm/rad)	800	600	400	200	100	50	**x**

Considered controllers: The intention of simulation 2 is to show how the two-layer control architecture performs for high-dof systems. To reduce the amount of figures that do not show any novel or different results, the choice is made to limit the results to FFL control.

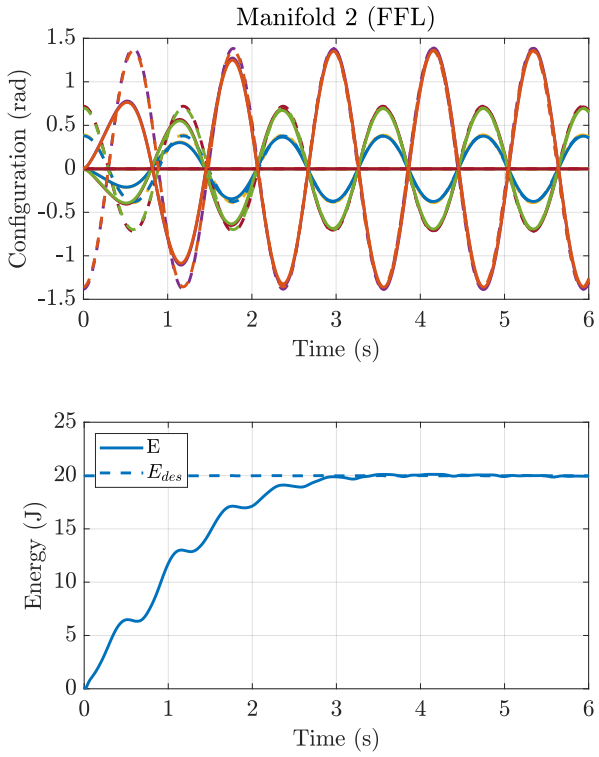

Fig. 12: Excitation of the 6-dof manipulator mode with the desired energy $E = 20J$ of the second Eigenmanifold. Each color corresponds to a different joint coordinate.

General performance: As seen in Figure 12, the results are similar to the double pendulum case, with convergence towards the virtual system achieved successfully. However, convergence time is considerably slower compared to the double pendulum. While this might be improved by more aggressive tunings of the trajectory reference controller, this would come at the cost of higher control efforts. Nonetheless, the simulation does highlight how the modular control architecture may be scaled to significantly more complicated systems without issues related to determining the Eigenmanifold parameterization. While only the second Eigenmanifold is shown, simulations for the other eleven Eigenmanifolds and energy levels showed similar results.

Modal switching: In Figure 13, the controller successfully brings the system to the new desired energy level. While the trajectory is non-smooth at the transition moment, the configuration variables stay stable in the transient period.

Simulation 3: Closed architecture fully actuated 6-dof manipulator

Here, the aim is to show that in the case of a closed architecture, where there is only access to joint-level reference control, similar theoretical guarantees for Eigenmode control may be presented using the two-layer architecture. Additionally, since we consider a fully actuated system, it becomes possible to

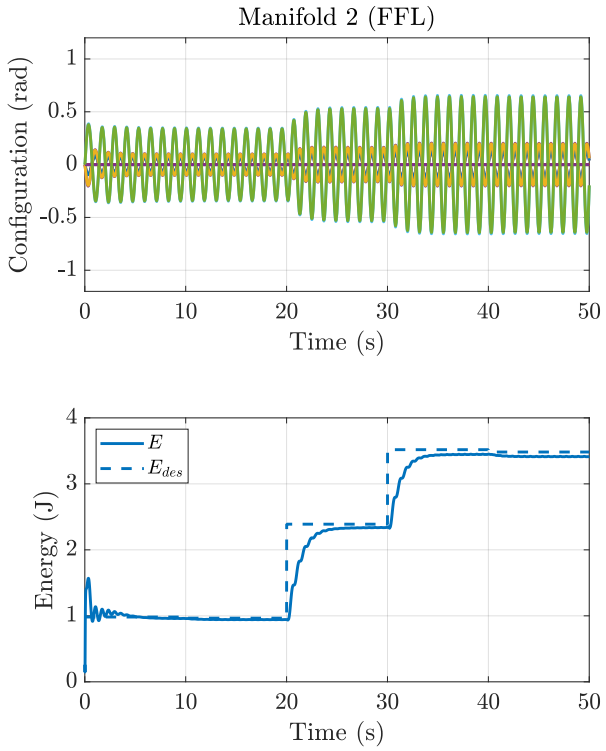

Fig. 13: Modal switching for the 6-dof series elastic joint manipulator.

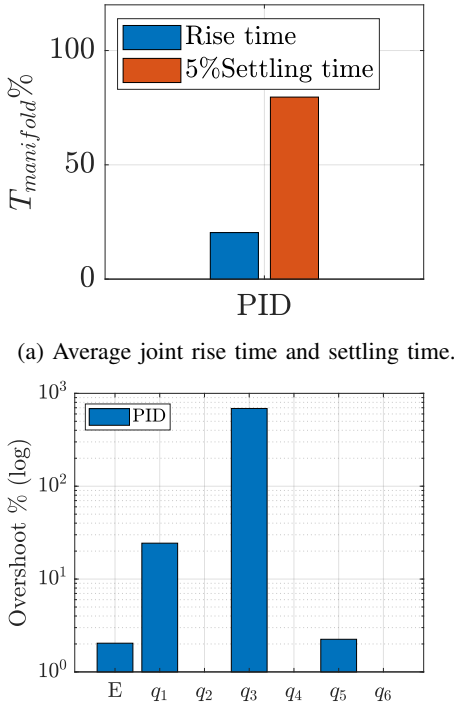

(a) Average joint rise time and settling time.

(b) Average energy and joint overshoot.

Fig. 14: Performance metrics for the closed-architecture manipulator for Eigenmanifold 4.

compare the control architecture with existing Eigenmanifold-based controllers. We conclude the case study by performing this comparative analysis.

Physical model: Consider a 6-dof manipulator with a stiff motor-link coupling, leaving a configuration manifold of $\mathfrak{X} \subseteq \mathbb{R}^6$, which is fully actuated. The equations of motion of this system can be described by (1) with a full-rank input coupling matrix $B(q) \in \mathbb{R}^{6\times 6}$. We assume rotational springs located in each joint with spring stiffness $k = [50, 50, 20, 20, 15, 5] Nm/rad$. Besides this, the system properties are identical to the elastically actuated case, and can be found in Table II.

Considered controllers: For the closed-architecture system, we consider a simple PID trajectory tracking controller described by (18) using the two-layer architecture. The PID controller is manually tuned with gains $K_p = 1Nm, K_d = 0.5Nm \cdot s, K_i = 1\frac{Nm}{s}$, where K_p, K_d, K_i respectively denote proportional, derivative and integral gain. A comparison is made with the standard PD-like Eigenmanifold controller presented in [9], which is defined as

$$\begin{aligned} u =& u_m + u_e \\ u_m =& M(q)\big(\alpha_p(q - Q(\xi_m) + \alpha_d(\dot{q} - \dot{Q}(\xi_m)\big) \\ u_e =& \gamma M(q)\big(E_d - E(q,\dot{q})\big)\dot{q} \end{aligned} \tag{19}$$

where α_p, α_d denote scalar proportional and derivative gains respectively and $(Q(\xi_m), \dot{Q}(\xi_m))$ denote the natural embeddings of $\mathfrak{M}$ into the tangent space $T\mathfrak{X}$, as explained in section II. The positive scalar γ denotes a gain for the energy regulating controller, where E_d is the desired energy of the system. The gains are manually tuned and are set to be $\alpha_p = 100\frac{1}{s^2}, \alpha_d = 8.5\frac{1}{s}, \gamma = 5\frac{1}{Js}$.

General performance: Figure 14 shows the performance metrics of the controllers in a similar fashion to simulation 1, with metrics again being collected and averaged over the excitation of a range of modes with energy levels from $E = 1J$ to $E = 15J$. Since the NNM trajectories of joints q_2, q_4, q_6 are zero, the percentage joint overshoot is not included due to singular values. Results are similar to simulation 1, with average rise time and settling time being shorter than a full manifold period. However, the configuration overshoot of joint q_3 is significantly larger in comparison to the other joints, being seven times higher. While no exact match, Figure 15 does show an initial overshoot of joint q_3, which is relatively large compared to the steady-state amplitude of the mode. Besides this, results do match the theory, with the control effort converging to zero and the system energy converging to the intended modal energy.

Global stability: Similar to simulation 1, the system is initialized from a number of different random states and tasked with tracking the $E = 1J$ NNM. Due to the increased complexity of the model, 32 initial conditions are tested, the results of which are shown in Figure 20. Even with the reduced sample size, results are similar to simulation 1. However, compared to the elastic joint simulation, the decrease is both slower and not exponentially convergent. This is expected, as the PID controller does not guarantee any degree of exponential convergence compared to FFL or SMC control. Results for modal switching are shown in Figure 18,

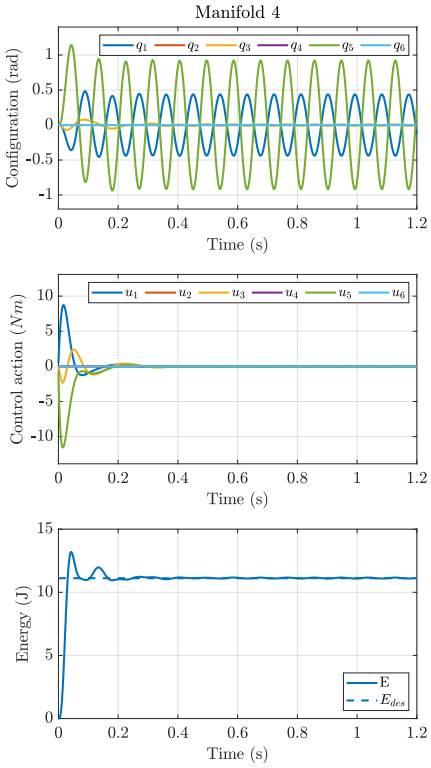

Fig. 15: Modal excitation of the NNM mode $E = 11J$ for the fully actuated manipulator using PID control.

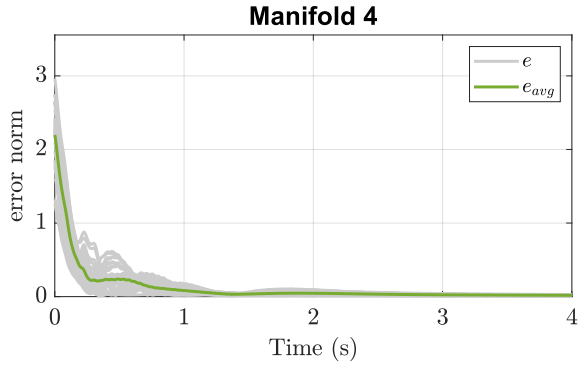

Fig. 16: Average error for the closed-architecture PID-controlled manipulator.

which match the other simulation results.

Comparison with PD-like Eigenmanifold control

To ensure fairness, the comparative analysis is performed on the same Eigenmanifold for both the PD-like controller and our proposed controller. A total of 32 simulations are performed with varying initial states sampled from $q(0) \in [-0.5\pi, 0.5\pi], \dot{q}(0) \in [-0.25\pi, 0.25\pi]$ for desired energy level $E = 1J$. As such, controller gains are manually tuned for optimal performance on $E = 1J$.

Global stability: Similar to previous simulations, Figure 19 displays the Euclidean normed distance to the Eigenmanifold over time. While the PD-like controller does not have global stability guarantees, the results indicate that in practice, the

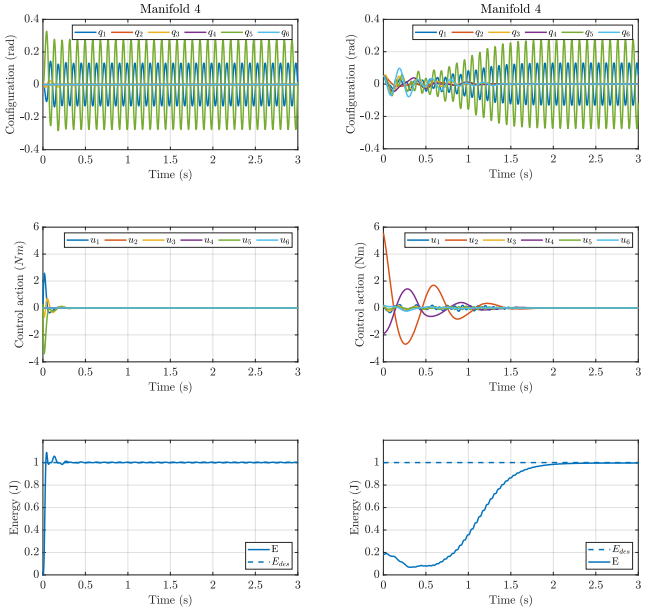

(a) PID two-layer architecture controller.

(b) PD-like Eigenmanifold controller [9].

Fig. 17: Excitation of the fully actuated 6-dof manipulator NNM with the desired energy $E = 1J$ of the fourth Eigenmanifold.

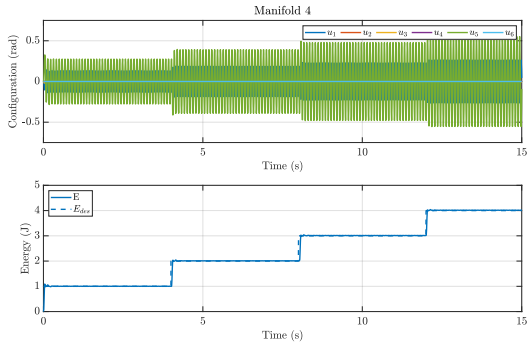

Fig. 18: Modal switching for the closed-architecture PID controller.

region of convergence is sufficiently large. When comparing this to Figure 20, the results are very similar, with asymptotic convergence successfully being achieved from every sampled initial state. While the mean normalized convergence time as shown in Table IV is larger by a factor 2.5, more aggressive tunings might improve this.

Modal switching: For modal switching, the desired modal energy is increased by $1J$ every 4 seconds. While the PD-like manifold controller is able to successfully switch and converge to low energy modes, instability occurs roughly at $E_{des} = 4J$. The mean energy (averaged over an interval of 5 times the manifold period) is also displayed, but does not achieve the desired energy. A possible explanation is that the energy regulating sub-controller and the Eigenmanifold stabilization sub-controller sufficiently interfere with each other, such that neither task is achieved. However, due to the lack of global stability guarantees for the controller, it is difficult to pinpoint

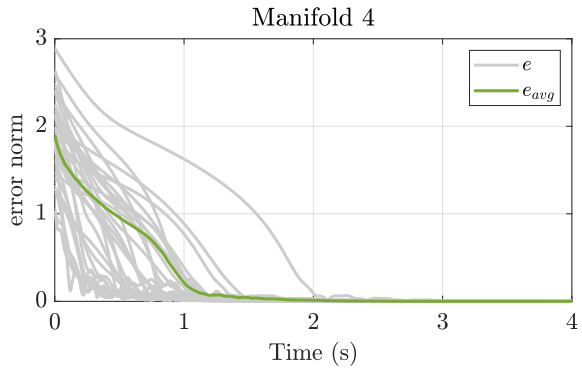

Fig. 19: Average error for the closed-architecture PD-like controlled manipulator.

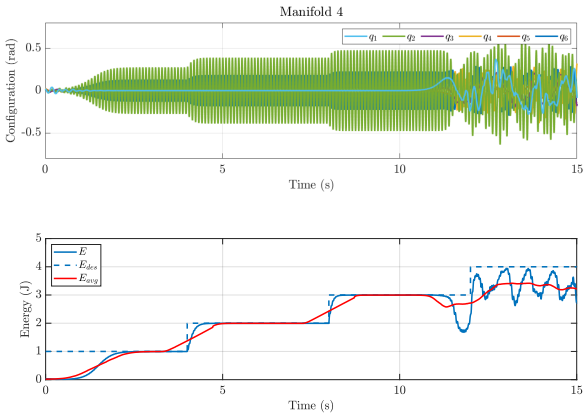

Fig. 20: Modal switching for the PD-like manifold controller.

the exact reason. To verify whether instability occurs due to inaccuracy of the Eigenmanifold estimation, the mean squared error between $Q(\xi_m)$ and the sample data used to estimate $\mathfrak{M}$ is calculated and shown in Table III, which implies that the accuracy of the Eigenmanifold estimation is not the cause of instability at energy levels above $E = 4J$. Another explanation for the failure is the locality of the Eigenmanifold parameterization, which is discussed in greater detail in Appendix B. Meanwhile, the two-layer architecture controller using PID tracking is able to perform stably where the PD-like controller fails, as seen in Figure 18. Additional simulations on modal switching have shown that this holds at least for excitation of modes with an energy level up until $E_{des} = 15J$.

TABLE III: Mean squared error of the manifold fit.

Conf. variable	MSE
q_1	$1.6223 \cdot 10^{-11}$
q_2	$7.5142 \cdot 10^{-24}$
q_3	$3.0620 \cdot 10^{-11}$
q_4	$3.3234 \cdot 10^{-23}$
q_5	$3.4418 \cdot 10^{-12}$
q_6	$2.8683 \cdot 10^{-23}$

Comparative table: We summarize the results of the comparative analysis in Table IV. Convergence time is calculated as the time at which the system energy is within 5% of the desired energy $E_{des} = 1J$ and the normalized error of all

TABLE IV: Results of comparative analysis.

Control method	PD-like[9]	Ours
Mean convergence time/T_{man}	6.9	2.0
Mean energy expenditure/$E(0)$	0.9932	1.808
Required parameterization	$(Q(\xi_m), \dot{Q}(\xi_m))$	$\mathfrak{R}(E)$
SEA control	no	yes
Globally provably stable	no	possible

configuration variables is less than 5% of the maximum normalized error over the entire time series. Energy expenditure is calculated as $\int_0^{T_t} \dot{q}^T(t)\tau dt(t)$ where T_t denotes the transient time. Due to the large variance in initial energy conditions, the energy expenditure is normalized through dividing by the initial energy $E(0)$.

The mean convergence time of the proposed two-layer architecture is significantly shorter. However, this comes at the cost of having an energy expenditure that is roughly twice as large during the transient period. Since both convergence time and energy expenditure are greatly impacted by the selected controller tunings, the absolute difference in performance cannot easily be measured. Nonetheless, our control method has distinct advantages, allowing for provable global stability and the excitation of modes in elastic joint robots. Furthermore, the two-layer architecture requires a less complex representation of the Eigenmanifold, which is advantageous for large-scale or complex systems. Since both considered control methods theoretically require zero control effort at steady state, the two-layer architecture is expected to be a better choice when the considered system bears any of the aforementioned properties. In the case that either control method can be employed, the choice is less straightforward.

Modal excitation for a planar n-joint link with an unactuated last link

In the previous section, we implied that the two-layer control architecture might be extended to more general classes of underactuated systems that allow a trajectory tracking controller. Here, we consider a three-link planar manipulator where the last link is unactuated, resulting in 1 degree of underactuation. A trajectory tracking controller is designed using partial feedback linearization, followed by a dynamic feedback linearization procedure on the remaining zero dynamics. For a detailed explanation and derivation, we refer back to [28]. The system dynamics are represented in the (local) coordinate system $q = [x_3, y_3, \theta]$, which denote the cartesian position of the root of the last link and its angle w.r.t. the ground in radians. Eigenmanifolds are calculated and described in this coordinate system. It is expected that calculating the modes in a global coordinate system and using Corollary 1 will yield similar results, with the modes more accurately representing the true modal behaviour of the system. However, theoretical proof and simulations for this are out of scope for the current work. Figure 21 displays the modal excitation of an arbitrary mode of the first Eigenmanifold. Convergence to the desired mode is clearly achieved, with the control effort disappearing when steady state is reached. Similar to previous findings, the initial control effort is unrealistically high, and would

require more careful controller tunings or some adaptive trajectory generation scheme to solve. Nonetheless, these results do indicate that the two-layer control architecture might be generalized to a larger class of underactuated systems.

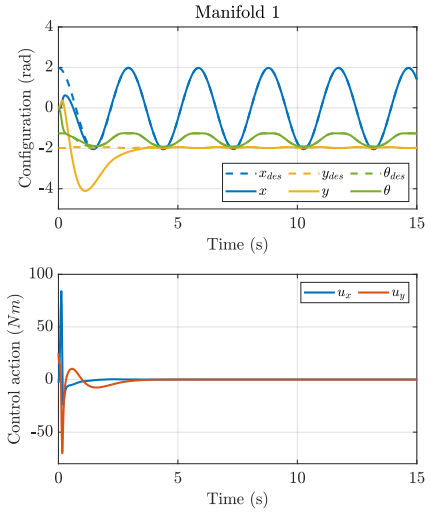

Fig. 21: Modal excitation for a three-link planar manipulator with an unactuated last link.

V. Discussion & future work

This paper introduced a modular control architecture that allows for NNM excitation of both series elastic joint robots and fully actuated conservative mechanical systems. Through rephrasing the Eigenmanifold control problem as trajectory tracking task, it becomes possible to employ existing trajectory control methods. This has opened up the way for controlling an additional class of systems, namely series elastic joint robots. While such systems are incompatible with existing Eigenmanifold control methods due to their underactuation, we have demonstrated through theory and numerical simulation that our proposed control architecture is successful in exciting NNMs of these elastic joint robots. Furthermore, we were able to dynamically generate modal reference trajectories using only the system equations of motion and the Eigenmanifold generator. Using a fully-actuated system, we compared our control architecture with more traditional Eigenmanifold-based control in simulation. While both control methods achieved similar levels of performance for lower energy levels, our proposed control architecture performed better at higher energy levels.

Although this direction is different compared to existing Eigenmanifold controllers, we believe the essence of modal control is present due to the explicit dependence on the geometric properties of the Eigenmanifold for the virtual system trajectory generation. Furthermore, the energy efficient properties, which are a main motivating factor for NNM control, are preserved.

A key advantage of the two-layer architecture is that only an accurate representation of the generator is needed, rather than the entire Eigenmanifold representation. Not only does this simplify offline computations, it also improves scalability. This is demonstrated in simulation by applying the architecture to a 6-degree-of-freedom manipulator. The control architecture is also compatible with fully actuated systems and does not require torque control, which allows for the application to closed-architecture robotic systems.

Good model knowledge is an unavoidable requirement for this architecture, but this is not a new restriction when compared to other Eigenmanifold-based controllers. While our work is so far limited to elastic joint robots and fully actuated robots, initial explorations suggest that this method can be applied to other unactuated systems permitting a trajectory tracking controller. We briefly discussed modal excitation on a dynamically feedback linearizable underactuated system. In future work, the extent to which trajectory-based Eigenmanifold control is generalizable can be investigated. Another promising research direction is the experimental validation of our control architecture on a physical elastic joint robot, as experimental results of applied Eigenmanifold control in the literature are limited.

The biggest limitation of this work is that the trajectory generator does not take into account the system state, which can cause the transient response of the system to have unrealistically high control inputs torques. Currently, avoiding this requires careful controller tuning and a slow increase in desired energy. A possible solution would be to introduce adaptive trajectory generation to counteract this behaviour, which can be explored in the future.

In summary, the two-layer architecture provides a new perspective and use-case for the application of Eigenmanifold-based control, without losing the important properties that make Eigenmanifold-based control beneficial. We believe this work is a first step in expanding the range of robotic systems for which Eigenmanifold-based control can be applied.

References

[1] Lorenzo Scalera et al. “Natural motion for energy saving in robotic and mechatronic systems”. In: *Applied Sciences* 9.17 (2019), p. 3516.

[2] Reinhardt Mathias Rosenberg. “Normal modes of nonlinear dual-mode systems”. In: (1960).

[3] Steven W Shaw and Christophe Pierre. “Normal modes for non-linear vibratory systems”. In: *Journal of sound and vibration* 164.1 (1993), pp. 85–124.

[4] Alin Albu-Schäffer and Cosimo Della Santina. “A review on nonlinear modes in conservative mechanical systems”. In: *Annual Reviews in Control* 50 (2020), pp. 49–71.

[5] Luigi Bono Bonacchi et al. “Efficient and goal-directed oscillations in articulated soft robots: the point-to-point case”. In: *IEEE Robotics and Automation Letters* 6.2 (2021), pp. 2555–2562.

[6] Davide Calzolari et al. “Single-Leg forward hopping via nonlinear modes”. In: *2022 American Control Conference (ACC)*. IEEE. 2022, pp. 506–513.

[7] Filip Bjelonic et al. “Experimental closed-loop excitation of nonlinear normal modes on an elastic industrial robot”. In: *IEEE Robotics and Automation Letters* 7.2 (2022), pp. 1689–1696.

[8] Pietro Pustina et al. “Nonlinear modes as a tool for comparing the mathematical structure of dynamic models of soft robots”. In: *2024 IEEE 7th International Conference on Soft Robotics (RoboSoft)*. IEEE. 2024, pp. 779–785.

[9] Cosimo Della Santina and Alin Albu-Schaeffer. “Exciting efficient oscillations in nonlinear mechanical systems through eigenmanifold stabilization”. In: *IEEE Control Systems Letters* 5.6 (2020), pp. 1916–1921.

[10] Cosimo Della Santina et al. “Using nonlinear normal modes for execution of efficient cyclic motions in articulated soft robots”. In: *Experimental Robotics: The 17th International Symposium*. Springer. 2021, pp. 566–575.

[11] Andre Coelho et al. “EigenMPC: An eigenmanifold-inspired model-predictive control framework for exciting efficient oscillations in mechanical systems”. In: *2022 IEEE 61st Conference on Decision and Control (CDC)*. IEEE. 2022, pp. 2437–2442.

[12] Cosimo Della Santina et al. “Exciting nonlinear modes of conservative mechanical systems by operating a master variable decoupling”. In: *2021 60th IEEE Conference on Decision and Control (CDC)*. IEEE. 2021, pp. 2448–2455.

[13] Marco Hutter et al. “Anymal-a highly mobile and dynamic quadrupedal robot”. In: *2016 IEEE/RSJ international conference on intelligent robots and systems (IROS)*. IEEE. 2016, pp. 38–44.

[14] Andy Abate and Jonathan W Hurst. “Oregon State’s CASSIE biped: Mechanical design for dynamic locomotion”. In: (2017).

[15] Alin Albu-Schäffer et al. “The DLR lightweight robot: design and control concepts for robots in human environments”. In: *Industrial Robot: an international journal* 34.5 (2007), pp. 376–385.

[16] Cliff Fitzgerald. “Developing baxter”. In: *2013 IEEE conference on technologies for practical robot applications (TePRA)*. IEEE. 2013, pp. 1–6.

[17] Reza Olfati-Saber. “Nonlinear control of underactuated mechanical systems with application to robotics and aerospace vehicles”. PhD thesis. Massachusetts Institute of Technology, 2001.

[18] Mark W Spong. “Modeling and control of elastic joint robots”. In: (1987).

[19] Alberto Isidori. “Elementary theory of nonlinear feedback for single-input single-output systems”. In: *Nonlinear Control Systems*. London: Springer London, 1995, pp. 137–217. ISBN: 978-1-84628-615-5. DOI: 10.1007/978-1-84628-615-5_5. URL: https://doi.org/10.1007/978-1-84628-615-5_5.

[20] Howard Georgi. *The physics of waves*. Prentice Hall, 2022.

[21] Gaëtan Kerschen et al. “Nonlinear normal modes, Part I: A useful framework for the structural dynamicist”. In: *Mechanical systems and signal processing* 23.1 (2009), pp. 170–194.

[22] Hassan K Khalil. *Nonlinear systems; 3rd ed.* The book can be consulted by contacting: PH-AID: Wallet, Lionel. Upper Saddle River, NJ: Prentice-Hall, 2002. URL: https://cds.cern.ch/record/1173048.

[23] Jingjing Jiang and Alessandro Astolfi. “Stabilization of a class of underactuated nonlinear systems via underactuated back-stepping”. In: *IEEE Transactions on Automatic Control* 66.11 (2020), pp. 5429–5435.

[24] Anton S Shiriaev, Leonid B Freidovich, and Sergei V Gusev. “Transverse linearization for controlled mechanical systems with several passive degrees of freedom”. In: *IEEE Transactions on Automatic Control* 55.4 (2010), pp. 893–906.

[25] Christian Fredrik Sætre et al. “Excessive transverse coordinates for orbital stabilization of (underactuated) mechanical systems”. In: *2020 European Control Conference (ECC)*. IEEE. 2020, pp. 895–900.

[26] Biao Lu, Yongchun Fang, and Ning Sun. “Continuous sliding mode control strategy for a class of nonlinear underactuated systems”. In: *IEEE Transactions on Automatic Control* 63.10 (2018), pp. 3471–3478.

[27] RB Gardner and WF Shadwick. “Feedback equivalence for general control systems”. In: *Systems & Control Letters* 15.1 (1990), pp. 15–23.

[28] Alessandro De Luca and Giuseppe Oriolo. “Trajectory planning and control for planar robots with passive last joint”. In: *The International Journal of Robotics Research* 21.5-6 (2002), pp. 575–590.

[29] Maxime Peeters et al. “Nonlinear normal modes, part II: Toward a practical computation using numerical continuation techniques”. In: *Mechanical systems and signal processing* 23.1 (2009), pp. 195–216.

[30] Jean-Jacques E Slotine, Weiping Li, et al. *Applied nonlinear control*. Vol. 199. 1. Prentice hall Englewood Cliffs, NJ, 1991.

[31] Sebastian Wolf, Oliver Eiberger, and Gerd Hirzinger. “The DLR FSJ: Energy based design of a variable stiffness joint”. In: *2011 IEEE international conference on robotics and automation*. IEEE. 2011, pp. 5082–5089.

APPENDIX A
TRAJECTORY TRACKING CONTROLLER DESIGN OF AN ELASTIC JOINT ROBOT

In this appendix, we will briefly show the procedure performed in [18] to develop a exact state-feedback linearizing controller for a SEA-driven manipulator with the equations of motion (3). Then, we prove the general lemma 1 for this specific application. First, substituting (3) into (16) gives

$$\begin{aligned}
y_1 =& T_{y1}(q,\dot{q}) = q_l \\
y_2 =& T_{y2}(q,\dot{q}) = \dot{q}_l \\
y_3 =& T_{y3}(q,\dot{q}) = \ddot{q}_l \\
=& -M(q_l)^{-1}(C(q_l,\dot{q}_l)\dot{q}_l + G(q_l) + K(q_l - q_m)) \\
y_4 =& T_{y4}(q,\dot{q}) = \dddot{q}_l \\
=& -\frac{d}{dt}M(q_l)^{-1}(C(q_l,\dot{q}_l)\dot{q}_l + G(q_l) + K(q_l - q_m)) \\
& - M(q_l)^{-1}\Big(\dot{q}_l\big(\frac{\partial C(q_l,\dot{q}_l)}{\partial q_l}\dot{q}_l \\
& - \frac{\partial C(q_l,\dot{q}_l)}{\partial \dot{q}_l}M(q_l)^{-1}\big(C(q_l,\dot{q}_l)\dot{q}_l + G(q_l) + K(q_l - q_m)\big) \\
& - C(q_l,\dot{q}_l)\big(M(q_l)^{-1}(C(q_l,\dot{q}_l)\dot{q}_l \\
& + G(q_l) + K(q_l - q_m)\big) + \frac{\partial G(q_l)}{\partial q_l}\dot{q}_l + K(\dot{q}_l - \dot{q}_m)\Big) \\
=& f_4(q_l, q_m, \dot{q}_l) + M(q_l)^{-1}K\dot{q}_m.
\end{aligned} \tag{20}$$

Here, $f_4(q_l, q_m, \dot{q}_l)$ collects all terms not related to $\dot{q}_m$ to simplify the notation.
To look at how the system evolves, we take the derivative

$$\begin{aligned}
\dot{y}_1 =& y_2 \\
\dot{y}_2 =& y_3 \\
\dot{y}_3 =& y_4 \\
\dot{y}_4 =& \frac{\partial f_4(q_l, q_m, \dot{q}_l)}{q_l}q_m \\
& + \frac{\partial f_4(q_l, q_m, \dot{q}_l)}{q_m} \\
& - M(q_l)^{-1}(C(q_l, q_m)q_m + G(q_l) + K(q_m - \dot{q}_l)) \\
& + \frac{\partial f_4(q_l, q_m, \dot{q}_l)}{\dot{q}_l}\dot{q}_m + \frac{d}{dt}M(q_l)^{-1}(K\dot{q}_m) \\
& + M(q_l)^{-1}K\Big(J^{-1}(q_l - \dot{q}_l) + J^{-1}u\Big) \\
=& F(q,\dot{q}) + M(q_l)^{-1}KJ^{-1}u
\end{aligned} \tag{21}$$

where $F(q,\dot{q})$ collects all terms not related to u. We can see that by setting u to be

$$u = -JK^{-1}M(q_l)F(q,\dot{q}) + JK^{-1}M(q_l)v \tag{22}$$

with $v \in \mathbb{R}^m$ defined as a new control input, the system transforms into a chain of four integrators

$$\begin{aligned}
\dot{y}_1 =& y_2 \\
\dot{y}_2 =& y_3 \\
\dot{y}_3 =& y_4 \\
\dot{y}_4 =& v
\end{aligned} \tag{23}$$

for which we can more easily design state-feedback control laws by defining v. We preserve a certain mechanical intuition of the system as this transformation implies that we can fully represent (3) using the position, velocity, acceleration, jerk, and snap of the joint coordinates q_l. However, although every exact state feedback linearizable system results in a chain of integrators, the output variable $y = \lambda(x)$ might not have any mechanical meaning for every system. Nonetheless, as long as the transformation is valid and defined in the region of a selected Eigenmanifold of the original system, the general structure and properties of the Eigenmanifold are preserved as implied by corollary 1, meaning we can exploit these properties in our new controller v.
While this derivation is shown specifically for (3), the same procedure holds true for any system that has a solution for the state space exact linearization problem. For more technical details for general systems, we refer back to [19].

A. Trajectory tracking

For an elastic joint manipulator, we can employ exact state-feedback linearization to develop an exponentially stable trajectory tracking controller using simple pole-placement control. If we then subsequently use the previously introduced reference trajectory $(q_d(t), \dot{q}_d(t)) = (q_m(t), \dot{q}_m(t))$, we show that the system state converges to the desired mode.
To show that this trajectory can be transformed into the new change of state variables and is still state-based, smooth, and viable, we present the following proposition.

Proposition 2. *Any nonlinear normal mode $(q_d(t), \dot{q}_d(t))$ of Eigenmanifold $\mathfrak{M}$ can be expressed in normal form of the system as $y_d(t)$ through application of map T_y, and its derivative $\dot{y}_d(t)$ is only dependent on the original state variables $(q_d(t), \dot{q}_d(t))$.*

Proof. While the initial statement of this proposition is trivially proven resulting from the fact that map T_y is globally defined, for completeness we briefly show this fact to be true. Recall that modal orbits are thus governed by the unforced evolution of (3) where $u = 0$ such that

$$\begin{aligned}
M(q_l)\ddot{q}_l + C(q_l,\dot{q}_l)\dot{q}_l + G(q_l) + K(q_l - q_m) = 0 \\
J\ddot{q}_m - K(q_l - q_m) = 0.
\end{aligned} \tag{24}$$

As transformation $T_y : (q,\dot{q}) \to y$ is globally defined, we apply this to the expression of the mode $(q_d(t), \dot{q}_d(t))$, resulting in

$$\begin{aligned}
y_{d1} =& q_{dl} \\
y_{d2} =& \dot{q}_{dl} \\
y_{d3} =& -M(q_{dl})^{-1}\Big(C(q_{dl},\dot{q}_{dl})\dot{q}_{dl} + G(q_{dl}) \\
& + K(q_{dl} - q_{dm})\Big) \\
y_{d4} =& f_4(q_{dl}, q_{dm}, \dot{q}_{dl}) + M(q_{dl})^{-1}K\dot{q}_{dm} \\
\dot{y}_{d4} =& F(q_d, \dot{q}_d).
\end{aligned} \tag{25}$$

Its derivative is defined as

$$\begin{aligned}\dot{y}_{d1} =& y_{d2}\\ \dot{y}_{d2} =& y_{d3}\\ \dot{y}_{d3} =& y_{d4}\\ \dot{y}_{d4} =& F(q_d, \dot{q}_d),\end{aligned} \tag{26}$$

where we see the dependency on u disappears for $\dot{y}_{d4}$, which is an important property which we can employ later in our control design to fully cancel out any nonlinearities through a feed-forward term. □

With this in mind, we present the following control candidate lemma:

Lemma 2. *Given the system described in* (3) *that permits an Eigenmanifold $\mathfrak{M}$ containing modes $(q_d(t), \dot{q}_d(t))$, with $i \in \mathbb{N}^+$ the controller*

$$\begin{aligned}u =& -JK^{-1}M(q_1)F(q,\dot{q}) + JK^{-1}M(q_1)v\\ v =& \dot{y}_{d4}(t) + k_1(y_{d1}(t) - y_1) + k_2(y_{d2}(t) - y_2)\\ &+ k_3(y_{d3}(t) - y_3) + k_4(y_{d4}(t) - y_4),\end{aligned} \tag{27}$$

where $[k_1, k_2, k_3, k_4]$ are negative definite gains chosen such that that all the poles of (23) *are negative definite and $y_d(t) = [y_{d1}, y_{d2}, y_{d3}, y_{d4}]^T$ denotes the nonlinear modes expressed in y by $T_y \circ (q_d(t), \dot{q}_d(t))$, will (exponentially) asymptotically stabilize the selected mode $(q_d(t), \dot{q}_d(t))$ expressed in q with the input u vanishing to zero, meaning*

$$\begin{aligned}\lim_{t\to\infty} q &= q_d(t)\\ \lim_{t\to\infty} \dot{q} &= \dot{q}_d(t)\\ \lim_{t\to\infty} u &= 0.\end{aligned} \tag{28}$$

Proof. Because y is linear, determining stability of the controller can be done by considering the eigenvalues of the closed-loop system. We take the error space of y by performing a linear change of coordinates $e(t) = y_d(t) - y$, which changes the system to

$$\begin{aligned}\dot{e}_1 =& e_2\\ \dot{e}_2 =& e_3\\ \dot{e}_3 =& e_3\\ \dot{e}_4 =& k_4e_4 + k_3e_3 + k_2e_2 + k_1e_1\end{aligned} \tag{29}$$

For stability, the eigenvalues of this system should be strictly negative, which can be checked by looking at $\det(e - \lambda) = 0$ which is

$$\lambda^4 - k_4\lambda^3 - k_3\lambda^2 - k_2\lambda - k_1 = 0 \tag{30}$$

From this, we gather that we can select any combination of $\{k_1, k_2, k_3, k_4\}$ which are positive and result in all negative eigenvalues. An example of this could be selecting gains such that the characteristic polynomial is equal to $(\lambda + 1)^4$, which would require gains $[k_1, k_2, k_3, k_4] = [-1, -4, -6, -4]$.
If all eigenvalues of (29) are negative, we may thus state

$$\begin{aligned}\lim_{t\to\infty} e &= 0\\ \lim_{t\to\infty} \dot{e} &= 0\\ \lim_{t\to\infty} y &= y_d(t)\\ \lim_{t\to\infty} \dot{y} &= \dot{y}_d(t).\end{aligned} \tag{31}$$

After applying the inverse map $T_y^{-1} \circ y$

$$\begin{aligned}\lim_{t\to\infty} q &= q_d(t)\\ \lim_{t\to\infty} \dot{q} &= \dot{q}_d(t),\end{aligned} \tag{32}$$

which we may insert into v as

$$\lim_{t\to\infty} v = \dot{y}_{d4}(t). \tag{33}$$

Taking the limit of the original control u, we then obtain

$$\lim_{t\to\infty} u = -JK^{-1}M(q_{dl})F(q_d, \dot{q}_d) + JK^{-1}M(q_{dl})\dot{y}_{d4}(t) \tag{34}$$

and thus

$$\begin{aligned}\lim_{t\to\infty} u =& -JK^{-1}M(q_{dl})F(q_d, \dot{q}_d)\\ &+ JK^{-1}M(q_{dl})F(q_d, \dot{q}_d)\\ =& 0,\end{aligned} \tag{35}$$

therefore showing that state $(q, \dot{q})$ indeed asymptotically converges to the selected mode $(q_d(t), \dot{q}_d(t))$ and that the input torque u simultaneously vanishes to zero. □

B. Sliding mode control

As sliding mode control is presented alongside full feedback linearization in the numerical validation section, we perform the same steps for a simple sliding mode controller. A procedure similar to [30] is applied.

Lemma 3. *Given the system described in* (3) *that permits an Eigenmanifold $\mathfrak{M}$ containing modes $(q_d(t), \dot{q}_d(t))$, the controller*

$$\begin{aligned}u =& -JK^{-1}M(y_1)\big(c_1(y_{d2} - y_2) + c_2(y_{d3} - y_3)\\ &+ c_3(y_{d4} - y_4) - F(y) + \dot{y}_{d4} + S\big)\\ S =& \epsilon sat(s) + \alpha s\\ s =& c_1(y_{d1} - y_1) + c_2(y_{d2} - y_2)\\ &+ c_3(y_{d3} - y_3) + (y_{d4} - y_4)\end{aligned} \tag{36}$$

where ϵ,α, c_1, c_2, c_3, c_4 are strictly positive scalars and $[y_{d1}, y_{d2}, y_{d3}, y_{d4}]^T = T_y \circ [q_d(t), \dot{q}_d(t)]^T$ denotes the selected normal mode expressed in the y state variables from (16)*, will asymptotically stabilize the selected mode $(q_d(t), \dot{q}_d(t))$ expressed in q with the input u vanishing to zero, meaning*

$$\begin{aligned}\lim_{t\to\infty} q &= q_d(t)\\ \lim_{t\to\infty} \dot{q} &= \dot{q}_d(t)\\ \lim_{t\to\infty} u &= 0.\end{aligned} \tag{37}$$

Proof. We start by once again introducing the change of state variables (16) to (3). In these new state variables, we introduce the time-varying surface

$$\begin{aligned}s(t) =& c_1(y_{d1} - y_1) + c_2(y_{d2} - y_2)\\ &+ c_3(y_{d3} - y_3) + (y_{d4} - y_4),\end{aligned} \tag{38}$$

which is invariant when $y = y_d(t)$, meaning $\dot{s}(t) = 0|_{y(t)\in y_d(t)}$. As such, the control problem can be rephrased to be

$$\lim_{t\to\infty} s(t) = 0, \tag{39}$$

which can be achieved exponentially by looking for the desired control behaviour

$$\dot{s}(t) = S(t) = -\big(\epsilon sign(t) + \alpha s(t)\big) \tag{40}$$

where ϵ and α are both strictly positive scalar gains. the discontinuous function $sign(s)$ is defined as

$$sign(s) = \begin{cases} 1 & , s > 0 \\ 0 & , s = 0 \\ -1 & , s < 0 \end{cases} \tag{41}$$

To circumvent possible chattering behaviour introduced by this function, we can replace $sign(s)$ by the continuous saturation function

$$sat(s) = \begin{cases} 1 & , s > 1 \\ s & , -1 \leq s \leq 1 \\ -1 & , s < 1 \end{cases} \tag{42}$$

Asymptotic stability of this behaviour for $s(t)$ can be verified by defining a Lyapunov function

$$V(s,t) = \frac{1}{2} s(t)^T s(t) \geq 0, \tag{43}$$

which is only equal to zero in the equilibrium point $s(t) = 0$. Then checking for the derivative

$$\begin{aligned} \dot{V}(s,t) =& -\big(\epsilon sat(s) + \alpha s\big)s \\ =& -\left(\epsilon sat(s)s + \alpha s^2\right) \leq 0|_{s(t)\neq 0} \end{aligned} \tag{44}$$

which shows asymptotical Lyapunov stability for $s(t) = 0$. However, since $V(s,t)$ is time-varying, we also need to look at the second derivative

$$\ddot{V}(s,t) = -(\epsilon sat(2s) - 2\alpha s) \tag{45}$$

which is bounded when $s(t)$ is bounded, and thus fulfills Barbalat's lemma [22]. Note that the statement $\frac{d}{dt} sat(s)s = sat(2s)$ can be trivially verified by writing out (42).
Then, looking at the derivative of $s(t)$, we obtain

$$\begin{aligned} \dot{s}(t) =& c_1(y_{d2} - y_2) + c_2(y_{d3} - y_3) \\ &+ c_3(y_{d4} - y_4) + \dot{y}_{d4} \\ &- F(y) + M(y_1)^{-1} K J^{-1} u, \end{aligned} \tag{46}$$

where $\dot{y}_4$ is replaced by the expression already derived in (21). Subsequently reordering this equation and inserting (40) results in the control law

$$\begin{aligned} u =& -JK^{-1}M(y_1)\big(c_1(y_{d2} - y_2) + c_2(y_{d3} - y_3) \\ &+ c_3(y_{d4} - y_4) - F(y) + \dot{y}_{d4} + S\big) \\ S =& \epsilon sat(s) + \alpha s \\ s =& c_1(y_{d1} - y_1) + c_2(y_{d2} - y_2) \\ &+ c_3(y_{d3} - y_3) + (y_{d4} - y_4) \end{aligned} \tag{47}$$

Subsequently verifying that $\lim_{t\to\infty} u = 0$ is done by setting $y = y_d(t)$ in (47) and seeing that all terms vanish in this case, thus concluding our proof. □

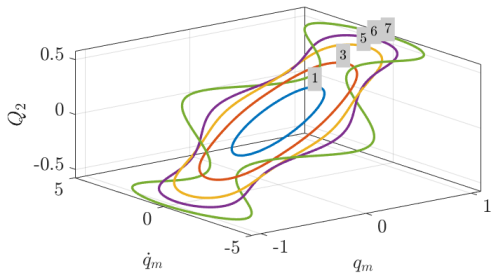

Fig. 22: A projection of the 1st Eigenmanifold of the system considered in simulation 3.

APPENDIX B
LOCALITY OF THE EIGENMANIFOLD PARAMETERIZATION

For the PD-like manifold controller, A closed parameterization ξ_m of the Eigenmanifold is required to calculate $(Q(\xi_m), \dot{Q}(\xi_m))$. A challenge which can occur at higher energy levels is the potential locality of ξ_m. In the simulations, the tangent parameterization as introduced in [4] is employed, with the parameterization being

$$\begin{aligned} \xi_m &= (q_m, \dot{q}_m) \\ q_m &= c^T q \\ \dot{q} &= c^T \dot{q} \end{aligned} \tag{48}$$

where c denotes the Eigenvector that defines an Eigenspace of the linearized system. Specifically, we assume that $\mathfrak{M}$ is a prolongation of this Eigenspace. However, as this is a local parameterization, only a subset of the full Eigenmanifold can be considered. This is illustrated in Figure 22, where self-intersection of the Eigenmanifold projection occurs at higher energy levels. To obtain a closed form parameterization of $\mathfrak{M}$, it subsequently becomes necessary to consider multiple tangent spaces to the Eigenmanifold, rather than only $q_m, \dot{q}_m$, increasing the complexity of the parameterization. Another natural parameterization of the Eigenmanifold is energy and arclength, but in this case at least two charts are required due to the S^1 topology of the arclength [4]. While Eigenmanifold-based controllers exist that do not require a closed parameterization of $\mathfrak{M}$ [7], our control method trivializes the entire problem by only requiring a projection of the generator $\mathfrak{R}$ into the tangent bundle $T\mathfrak{X}$.